Water Research 157 (2019) 106–118

Contents lists available at ScienceDirect

Water Research

journal homepage: www.elsevier.com/locate/watres

Catalyst-free activation of persulfate by visible light for water disinfection: Efficiency and mechanisms

Wanjun Wang [a], Hanna Wang [a], Guiying Li [a], Taicheng An [a, *], Huijun Zhao [b], Po Keung Wong [c, **]

[a] Guangzhou Key Laboratory of Environmental Catalysis and Pollution Control, Guangdong Key Laboratory of Environmental Catalysis and Health Risk Control, School of Environmental Science and Engineering, Institute of Environmental Health and Pollution Control, Guangdong University of Technology, Guangzhou, China
[b] Centre for Clean Environment and Energy, and Griffith School of Environment, Gold Coast Campus, Griffith University, Queensland, 4222, Australia
[c] School of Life Sciences, The Chinese University of Hong Kong, Shatin, NT, Hong Kong, China

ARTICLE INFO

Article history:
Received 15 November 2018
Received in revised form
24 February 2019
Accepted 1 March 2019
Available online 28 March 2019

Keywords:
Water disinfection
Persulfate
Sulfate radical
Visible light
Catalyst-free

ABSTRACT

The development of cost-effective water disinfection methods is highly desired to address the problems caused by outbreak of harmful microorganisms. Sulfate radical ($\bullet SO_4^-$)-based advanced oxidation technology has attracted increasing attention. However, various catalysts or UV irradiation are usually used to activate persulfate (PS), which is high-cost and the recovery of nano-sized catalysts is also challenging. This work demonstrates a new method of catalyst-free activation of persulfate by visible light (VL) for bacterial inactivation. The 6-log of *E. coli* cells can be inactivated within 40 min and 7-log of *E. coli* cells could be inactivated within 120 min by the VL/PS system. The major responsive wavelength is 420 nm, and no heat activation of PS is found during VL irradiation. A synergistic effect with synergy factor of 51.2% is found when combining the VL irradiation with heating at 50 °C. The acidic pH is benefit for the VL/PS-triggered bacterial inactivation, while bicarbonate inhibits the *E. coli* inactivation at the range of 0.1–20 mg/L. Mechanism study indicates the main reactive species are $\bullet SO_4^-$, $\bullet O_2^-$ and •OH, in which $\bullet SO_4^-$ plays the most important role. The bacterial inactivation process shows to begin from outer membrane to intracellular components. Subsequently, the antioxidant enzyme (i.e. SOD, CAT) is induced, followed by damaging to the genomic DNA leading to fatal death of the cells. In addition, the VL/PS system is also applicable for the inactivation of other pathogenic bacteria, including *Staphylococcus aureus* and *Pseudomonas aeruginosa*, showing universality for water disinfection applications. This work not only provides a new cost-effective disinfection method without a catalyst, but also sheds light on understanding the bacterial inactivation mechanism by $\bullet SO_4^-$-based AOPs.

1. Introduction

Depletion of water quality due to contamination of water bodies by recalcitrant compounds and microbial pathogens has become a serious global problem with increasing populations and uncertain global climate changes. In efforts to improve water quality, the inactivation of waterborne pathogens for provision of safe potable water has been taken as a priority in health programs, as huge occurrence of mortality especially in developing countries originating from microbial contaminated water (Catley-Carlson, 2017; Montgomery and Elimelech, 2007; Wang et al., 2017). Traditional water disinfection methods such as chlorination, ozonation and UV irradiation have many drawbacks and associated disadvantages (Dalrymple et al., 2010; Wang et al., 2015). For example, a number of microorganisms are resistant to UV irradiation and chlorination (Anastasi et al., 2013; Haaken et al., 2013; Rizzo et al., 2013); the high-cost and safety concerns of ozonation limit its practical application (Sichel et al., 2007); the formation of carcinogenic disinfection byproducts (DBPs) by chlorination and ozonation has become another serious environmental problem (Lu et al., 2018; Parker et al., 2014). Therefore, more safe and "green" water disinfection technologies are highly desired to achieve cost-effective inactivation of pathogens and elimination of disinfection debris.

* Corresponding author.
** Corresponding author.
E-mail addresses: antc99@gdut.edu.cn (T. An), pkwong@cuhk.edu.hk (P.K. Wong).

https://doi.org/10.1016/j.watres.2019.03.071
0043-1354/

In recent decades, hydroxyl radical (•OH) based advanced oxidation processes (AOPs), such as Fenton, photo-Fenton, and electro-Fenton, have been widely investigated to be effective for the degradation of pollutants (Babuponnusami and Muthukumar 2012; Brillas et al., 2009; Giannakis et al., 2018). Nevertheless, huge amount of sludge, low optimal reaction pH, difficulties in the storage and transport of H_2O_2 still remain challenges (Guo et al., 2018; Luo et al., 2014). Recently, AOPs based on sulfate radical ($\bullet SO_4^-$) have attracted increasing attention because of its strong redox potential (2.5–3.1 V) similar to •OH (Guan et al., 2011). Under neutral or basic pH conditions, $\bullet SO_4^-$ can be converted to •OH, which exhibits a slightly higher redox potential than $\bullet SO_4^-$ (Liang et al., 2007). The half-life of the $\bullet SO_4^-$ (30–40 μs) is generally longer than that of •OH (less than 1 μs) (Farhat et al., 2015; Zhao et al., 2017). In addition, compared to liquid H_2O_2, the solid persulfate (PS) is cheaper ($0.74/kg vs $1.5/kg of H_2O_2), more chemically stable, and more convenient to transport, store, and use in various applications (Duan et al., 2015). $\bullet SO_4^-$ based AOPs have been widely used for the degradation of various emerging organic pollutants, such as atrazine (Khan et al., 2017), carbamazepine (Liu et al., 2018), ampicillin (De Luca et al., 2017), etc. Recently, it has also been extended to the application of microorganism inactivation. For instance, Michael-Kordatou et al. (2015) have used UVC to activate PS for the inactivation of erythromycin (ERY)-resistant *Escherichia coli* cells, and total inactivation can be achieved within 90 min. Furthermore, natural pyrrhotite has also been found to be able to activate PS to produce $\bullet SO_4^-$ for the inactivation of *Escherichia coli* and *Staphylococcus aureus*, which was attributed to the Fe(II)-mediated activation of PS (Xia et al., 2017).

Generally, PS activation can be initiated by physical methods such as UV irradiation, microwave and heating (An et al., 2015; Qi et al., 2017), or by chemical methods such as transition metals (e.g. Fe^0, Fe^{2+}, Cu^{2+}, Ag^+), bases, phenols, and quinones (Ahmad et al., 2013; Fang et al., 2013; Wang and Wang, 2018). Recently, heterogeneous PS activation has been explored and various catalysts have been developed, such as transition metal-based catalysts (e.g. Fe_3O_4, CuO, Co_3O_4, etc.) (Du et al., 2017; Liang et al., 2012; Zhao et al., 2015) and metal-free carbonaceous materials (carbon nanotube, graphene and nanodiamond, etc.) (Duan et al. 2015, 2016b; Kang et al., 2016; Lee et al., 2015). However, limitations for wide application of these catalysts still exist. For example, the complexity and mass production of these catalysts increase the practical application costs. In addition, the potential leakage of heavy metal ions (such as Co^{2+} and Cu^{2+}) or other elements in the catalysts would cause secondary environmental pollution (Gao et al., 2017). Therefore, PS activation without the use of a catalyst is highly desired from the practical use point of view. Fortunately, sunlight has provided us an ideal and inexhaustible energy source for the PS activation. However, most of the present studies have only focused on UV irradiation for PS activation, which accounts for only 5% of the sunlight spectrum, while about 48% of the sunlight energy is in visible light (VL) region. But no studies have been conducted the VL-driven PS activation without catalyst for the application of bacterial inactivation even to insight into its underlying mechanisms. Therefore, it is very attractive to develop cost-effective VL/PS systems and study the feasibility for water disinfection.

Herein, catalyst-free visible-light-irradiation was firstly utilized to activate PS for *Escherichia coli* inactivation, a model bacterial strain in water. The efficiency and feasibility of using the VL/PS system for bacterial inactivation was evaluated in terms of light wavelength, cell density, temperature, pH, bicarbonate, etc. The bacterial inactivation mechanisms in terms of major radical species and their roles in inactivation process were also studied. Several antioxidant enzymes, intracellular reactive oxygen species (ROSs) and chromosomal DNA destruction were monitored during the treatment process, and finally a possible bacterial inactivation mechanism was proposed. Moreover, the universality of VL/PS system for inactivating other pathogenic bacteria was also attempted. As a proof-of-concept, this work may provide useful information on developing simple and cost-effective method for the inactivation of pathogenic microorganism in water-scarce regions using the inexhaustible sunlight as the energy source.

2. Experimental section

2.1. Chemicals

Potassium persulfate (PS), 5,5-dimethyl-1-pyrroline *N*-oxide (DMPO), 4-hydroxy-2,2,6,6-tetramethylpiperidin-1-oxyl (TEMPOL) and coumarin were purchased from Aladdin, China. Bicarbonate ($NaHCO_3$), *tert*-butyl alcohol (TBA) were obtained from Damao Chemical Reagent, China. Methanol was purchased from Guangzhou Chemical Reagent, China. All the reagents were analytical grade and prepared in ultrapure water (Millipore, Molsheim France).

2.2. Experimental procedure

E. coli was chosen as the model bacteria to evaluate the inactivation ability of the VL/PS system (Wang et al., 2018). In a typical experiment, bacterial cells were cultured in Nutrient Broth growth medium at 37 °C with shaking, and then harvested in the late exponential phase of growth. The harvested bacteria were centrifuged at 8000 rpm for 1 min, and the pellets were then washed with sterilized saline (0.9% NaCl) solution three times in a centrifuge tube and re-suspended in a sterilized saline solution to obtain suitable concentration of *E. coli*. Then, PS with different concentrations was added into 100 mL solution containing 10^7 cfu mL^{-1} bacterial suspensions. The solution was irradiated by a 300 W Xenon lamp equipped with a 420 nm cut-off filter. The VL irradiation was measured by a photometer (FZ-A, PerfectLight, China) to be 220 mW/cm^2. In order to study the effect of wavelength, the different monochromatic light (420, 450 and 550 nm) was used and the irradiation was adjusted to the same level of 35 mW/cm^2. At different time intervals, aliquot samples were collected and uniformly spread on Nutrient Agar plates after serial dilutions using the sterilized saline solution. The plates were incubated at 37 °C for 24 h to determine the viable cell count. All the inactivation experiments were conducted in triplicate. The system temperature maintained at about 30 °C during the inactivation process. Control experiments without light irradiation were also conducted in triplicate. The effects of different PS concentrations, bacterial concentrations, temperatures and pH values were also studied. To analyze the influence of pH, appropriate amounts of H_2SO_4 (0.1 M) or NaOH (0.1M) was added to adjust the initial pH value. To test the universality, Gram-positive *Staphylococcus aureus* and Gram-negative *Pseudomonas aeruginosa* were also used, following similar experimental procedure as *E. coli*.

2.3. Analysis

Sulfate radical was tested using Electron Paramagnetic Resonance (EPR) technology. Typically, a solution containing 10 mM DMPO and 2 mM PS was prepared and irradiated by visible light ($\lambda \geq 420$ nm). After given time intervals, aliquots were collected and analyzed on a Bruker EMXPlus EPR spectrometer. The •OH production was monitored using coumarin as the trapping agent. A solution containing 1 mM coumarin, 2 mM PS was prepared and irradiated with different light conditions. At given time intervals, aliquots were taken and measured by a Fluorescence spectrometer at an emission wavelength of 460 nm with an excitation

wavelength at 332 nm. Intracellular enzyme protein was extracted by Bacterial Protein Extraction Kit (C600596,Sangon Biotech), then analyzed by Total Superoxide Dismutase Assay Kit with WST-8 (S0101,Boyotime) and Catalase Assay Kit (S0051,Boyotime) to test the enzyme activity. PS concentration was measured using the KI colorimetric method at 400 nm according to reported method (Liang et al., 2008; Liu et al., 2014; Feng et al., 2015) with a Varian Cary 500 UV-vis spectrophotometer. Intracellular reactive oxygen species were detected by Reactive Oxygen Species Assay Kit with fluorescent probe DCFH-DA (S0033, Boyotime). Chromosomal DNA was extracted using an Ezup Column Bacteria Genomic DNA Purification Kit (SK8255, Sangon Biotech), then verified by DNA agarose gel electrophoresis (0.6% agarose gel at 100 V for 30 min in 1 × TAE buffer).

3. Results and discussion

3.1. Bacterial inactivation efficiency by VL/PS system

The inactivation profiles of different concentrations of *E. coli* against the reaction time with PS under VL irradiation ($\lambda \geq 420$ nm) are shown in Fig. 1(A). The VL spectrum is shown in Fig. S1, which shows that no UV irradiation is found. Fig. 1(A) shows that PS alone has no bactericidal effect on different concentrations of *E. coli*, indicating PS cannot be activated by bacterial cells under dark conditions. Impressively, under VL irradiation, remarkable bacterial inactivation efficiency was obtained with PS addition. 6 log of *E. coli* cells could be completely inactivated within 40 min, and 7 log of *E. coli* cells could be inactivated within 120 min of VL irradiation with 2 mM PS. When the bacterial concentration was further increased to 10^8 cfu mL^{-1}, about 4-log reduction of viable cells could still be achieved within 120 min. The inactivation under full spectrum irradiation was also conducted to evaluate the effect of solar light activated PS for disinfection. As expected, the inactivation efficiency was further enhanced and 7 log of cells could be inactivated within 40 min, suggesting PS can also be used to accelerate the solar disinfection (SODIS) process without catalysts, in which both UV and VL play important role in activating the PS for disinfection. In addition, the bacterial inactivation efficiency was closely related to the PS concentration in the PS/VL system. Negligible inactivation efficiency was found when the PS concentration was 0.5 and 1 mM. When the PS concentration was increased to 2 mM, the inactivation efficiency was greatly improved and 7-log reduction of viable cells could be achieved within 120 min of VL irradiation (Fig. 1(B)). Further increasing the PS concentration would also lead to increase of inactivation efficiency, and total inactivation of 7-log *E. coli* cells could be achieved within 80 min when the PS concentration was increased to 4 mM. During the bacterial inactivation process in the VL/PS system, the decrease of system pH was observed and became more obvious with increasing PS concentration as shown in Fig. 1(C). When the PS concentration was 4 mM, the pH was decreased from 6.0 to 4.6 after the complete

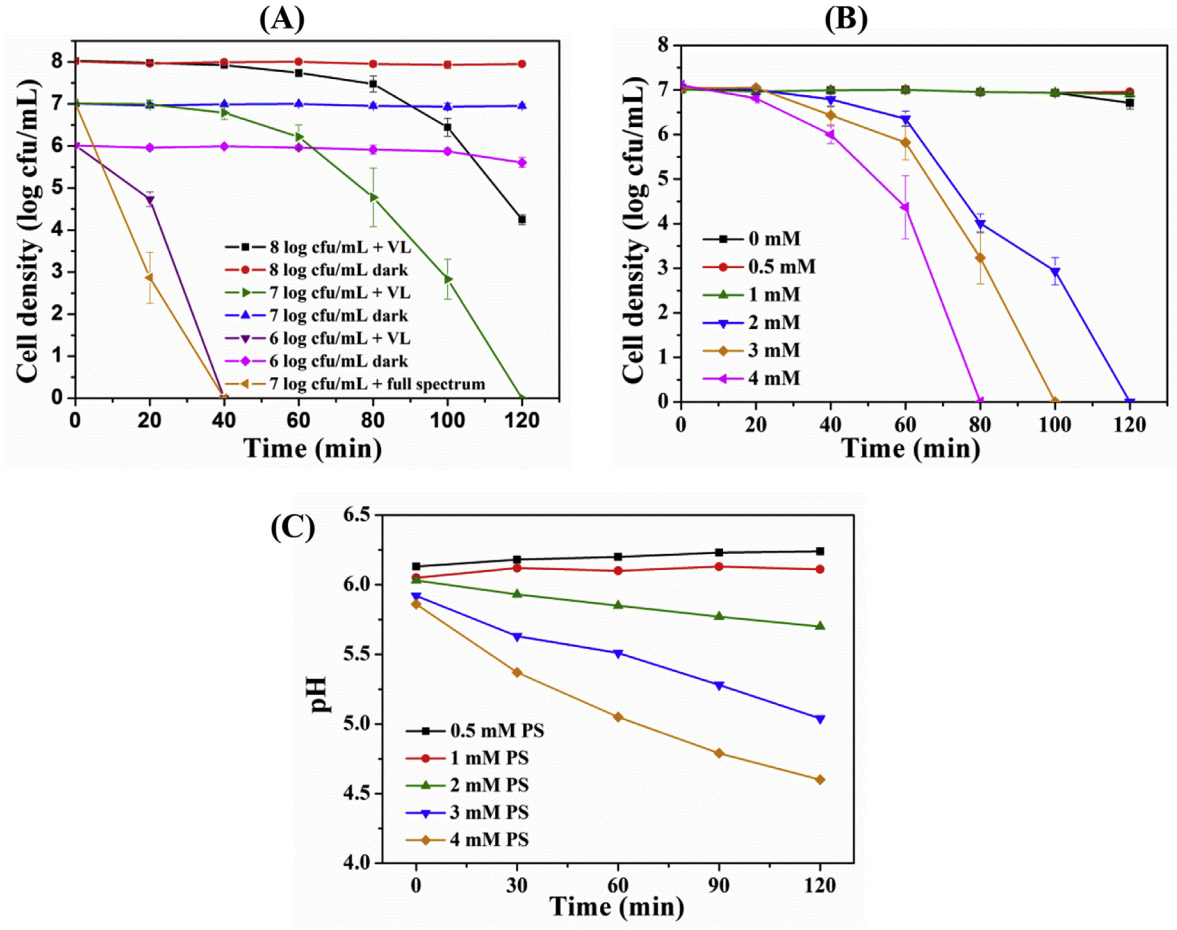

Fig. 1. (A) Sulfate radical-mediated bacterial inactivation efficiency in the VL/PS system with different cell densities ($\lambda \geq 420$ nm; [PS] = 2 mM; T = 30 °C; $[pH]_0 = 6.0$); (B) Bacterial inactivation efficiency in the VL/PS system with different PS concentrations and (C) Variation of pH values during the inactivation in the VL/PS system (cell density = 7 log cfu mL^{-1}; T = 30 °C; $[pH]_0 = 6.0$).

bacterial inactivation. The reason for the pH decrease may be partially due to H^+ generation during the process of $\bullet SO_4^-$ consumption (Equation (1)) (Liu et al., 2012).

$$\bullet SO_4^- + H_2O \rightarrow SO_4^{2-} + \bullet OH + H^+ \quad (1)$$

In addition, the endo and exo-bacterial organic compounds attacked by $\bullet SO_4^-$-derived ROSs would release aliphatic acids, which also contributed to the pH decrease (Rincon and Pulgarin, 2004a). Previous studies have confirmed that PS can be activated by UV irradiation (254 nm or 365 nm) for organic pollutants degradation (Antoniou et al., 2010; Liu et al., 2016). However, studies about PS activation by VL are rather limited. Pan et al. (2018) have investigated the light activation of PS for benzophenone-3 degradation, and the results showed that the degradation ratio was low (~20%) under pure VL irradiation ($\lambda = 420$ nm). Our present results confirm that PS can also be activated by VL for high-efficient bacterial inactivation without any artificial catalysts.

To further evaluate the effectiveness of bacterial inactivation in the VL/PS system, bacterial regrowth test was conducted according to the method reported in the literatures (Wang et al., 2012; Rincon and Pulgarin, 2004b). After the complete inactivation of 7-log *E. coli* cells in 120 min (Fig. 1(A)), the reaction mixture (1 mL) was sampled in the culture medium (20 mL) and underwent a 96 h recovery period in dark to determine the bacterial regrowth. Results indicated that no detectable bacterial count was observed after 96 h incubation period, suggesting the bacterial inactivation by the VL/PS system lead to irreversible damage to the *E. coli* cells. Thus, the VL/PS treatment is a safe and effective method for water disinfection without detectable bacterial regrowth.

To understand the mechanisms, the responsive wavelength in the VL region for bacterial inactivation were investigated. Fig. 2(A) shows the wavelength-dependent bacterial inactivation efficiency under monochromatic light irradiation with different band-pass filter. No UV irradiation was found in the monochromatic light spectra, confirming the purity of the monochromatic light (Fig. S1). Results show that a high bacterial inactivation efficiency was found at 420 nm light irradiation, and 7-log reduction of viable cells could be achieved within 120 min. When extending the light wavelength to 450, 550 and 650 nm, the bacterial inactivation efficiency was decreased significantly, indicating the responsive wavelength in the visible light region is around 420 nm. As well known, sulfate radical reacts with hydroxide or water to produce hydroxyl radical (•OH) (Furman et al., 2010; Gao et al., 2016b). Therefore, to further confirm the PS can be activated under VL irradiation, •OH production was monitored using coumarin as the trapping agent. Coumarin is believed to quantitatively react with •OH to produce highly fluorescent 7-hydroxylcoumarin with emission at 460 nm (Guan et al., 2008; Ishibashi et al., 2000; Ng et al., 2015). Fig. 2(B) shows the fluorescence spectra of the coumarin solution (1 mM) in the presence of PS under 420 nm of VL irradiation. It was found that the fluorescence intensity of 7-hydroxylcoumarin increased with irradiation time, suggesting PS can be activated to produce •OH under 420 nm VL irradiation. In addition, the apparent rate constant (k) for •OH generation was calculated following pseudo-first-order reaction kinetics based on previous literatures (Guan et al., 2008). As shown in Fig. 2(C), the generation of •OH increases linearly under 420 nm irradiation with apparent rate constant $k = 0.2522$ min^{-1} ($R^2 = 0.992$). When the light wavelength was extended to longer wavelength of 450, 550, and 650 nm, the •OH generation gradually decreased almost to zero. This result matches well with the bacterial inactivation efficiency, suggesting the bacterial cells were inactivated as a result of PS activation to produce reactive species. It should be noted that slight •OH generation could be found under 450 nm of VL irradiation ($k = 0.0469$ min^{-1}, $R^2 = 0.994$). However, almost no bacterial inactivation was obtained under this wavelength, which indicates that PS may also be activated under longer wavelength in the VL region ($\lambda \geq 450$ nm), but the generated reactive species are limited and unable to cause cell death. To further confirm the activation of PS, the consumption of PS was studied and the results were shown in Fig. 2(D). It was found that ~40 mg/L of PS (~7.8%) was decomposed under VL irradiation ($\lambda \geq 420$ nm) during the bacterial inactivation process, which followed a first-order reaction kinetic model ($k_{ps} = 6.86 \times 10^{-4}$ min^{-1}, $R^2 = 0.995$). In addition, similar PS consumption rate was found under 420 nm irradiation, while negligible PS was consumed under 450 nm and 550 nm irradiation. This result matched well with the bacterial inactivation efficiency in Fig. 2(A), further confirming the bacterial inactivation is caused by the consumption of PS with VL irradiation.

To illuminate the roles of possible reactive species, different scavengers were used to trap potential reactive species in the VL/PS system, including methanol for $\bullet SO_4^-$, *tert*-butyl alcohol (TBA) for •OH and TEMPOL for $\bullet O_2^-$ (Duan et al., 2016a; Liu et al., 2014; Wang et al., 2011). In the control experiment without PS, no bacterial cell loss was observed by adding 1 mM of each scavenger, indicating no toxicity of these chemical scavengers to the *E. coli* cells within the testing time period (Fig. S2). It is known that methanol can effectively scavenge both $\bullet SO_4^-$ and •OH, while TBA is more efficient to scavenge •OH than that of $\bullet SO_4^-$ ($k_{\bullet OH} = 5.2 \times 10^8$ M^{-1} s^{-1}; $k_{\bullet SO4}^- = 8.4 \times 10^5$ M^{-1} s^{-1}) (Ahmad et al., 2013). As shown in Fig. S3, with the addition of methanol, the inactivation of bacteria was almost completely quenched, indicating the major reactive species in the VL/PS system are $\bullet SO_4^-$ or •OH. In contrast, the addition of TBA only partially decreased the inactivation efficiency, suggesting both $\bullet SO_4^-$ and •OH are involved in the bacterial inactivation process. The $\bullet SO_4^-$ has both direct functions to cause cell death and indirect function by producing •OH to oxidize the cells. Furthermore, it was also found that the addition of TEMPOL could inhibit the bacterial inactivation, suggesting $\bullet O_2^-$ also played an important role during the inactivation process. Furman et al. has indicated that PS can be activated by base and decomposed to sulfate and hydroperoxide anion (HO_2^-), then the hydroperoxide anion reduces another PS molecule resulting in the formation of sulfate radical and sulfate while the hydroperoxide is oxidized to superoxide (Furman et al., 2010). Therefore, it is found that PS can also be activated by VL to produce $\bullet O_2^-$. Based on the above results, the mechanisms in the VL/PS system go through the following reactions (Equations (2)–(4)):

$$^-{}_3OS\text{-}O\text{-}O\text{-}OS_3^- + H_2O \rightarrow 2SO_4^{2-} + HO_2^- + H^+ \quad (2)$$

$$^-{}_3OS\text{-}O\text{-}O\text{-}OS_3^- + HO_2^- \rightarrow SO_4^{2-} + \bullet SO_4^- + \bullet O_2^- + H^+ \quad (3)$$

$$\bullet SO_4^- + H_2O \rightarrow SO_4^{2-} + \bullet OH + H^+ \quad (4)$$

The key step for the activation of PS is the generation of $\bullet SO_4^-$, therefore further tested experiments for the generation of $\bullet SO_4^-$ by EPR spectroscopy was also conducted using DMPO as a spin-trapping reagent (Wei et al., 2017; Zhu et al., 2016). Fig. 3 shows the obvious signals of both DMPO-•OH (1:2:2:1) and DMPO-$\bullet SO_4^-$ (1:1:1:1:1:1), indicating large quantities of both •OH and $\bullet SO_4^-$ radicals were generated immediately in the VL/PS system. The signals corresponding to •OH became more pronounced with irradiation time, suggesting the conversion of $\bullet SO_4^-$ to •OH. These results confirm the successful activation of PS by VL to produce $\bullet SO_4^-$, •OH and $\bullet O_2^-$, which then collectively cause the inactivation of bacterial cells.

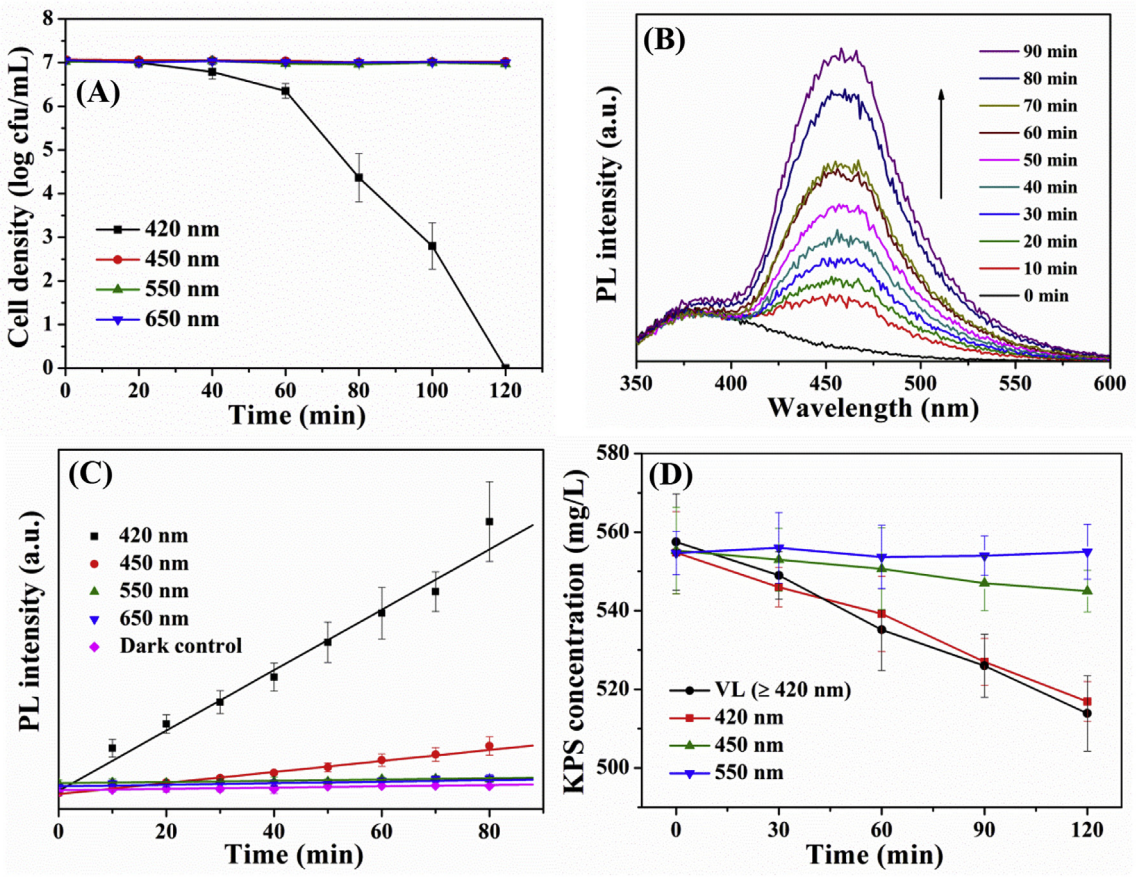

Fig. 2. (A) Bacterial inactivation efficiency under different monochromatic light irradiation; (B) Fluorescence spectra of coumarin solution (1 mM) in the presence of PS under 420 nm of VL irradiation; (C) Fluorescence intensity at 460 nm under different monochromatic light irradiation; (D) PS consumption during the bacterial inactivation process under different VL wavelengths. Experimental conditions: cell density = 7 log cfu mL^{-1}; [PS] = 2 mM; T = 30 °C; $[pH]_0$ = 6.0.

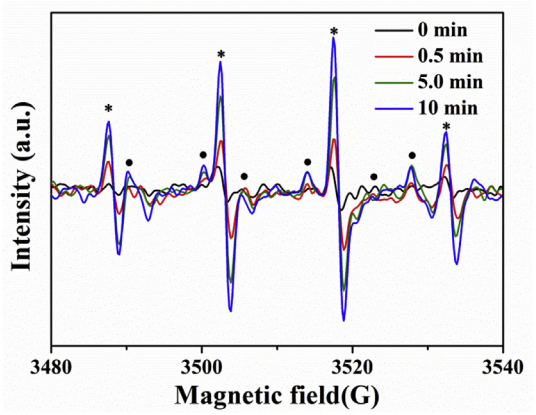

Fig. 3. Electron paramagnetic resonance (EPR) spectra of DMPO spin-trapping adducts (asterisk represent DMPO-•OH, and circle represent DMPO-•SO_4) in the VL/PS system. Experimental conditions: λ ≥ 420 nm; [PS] = 2 mM; T = 30 °C; $[pH]_0$ = 6.0.

3.2. Influences of several factors to VL/PS system

3.2.1. Effect of temperature for PS activation

As well known, PS can be activated by heat (Ike et al., 2018; Waldemer et al., 2007; Zrinyi and Pham, 2017). Since VL irradiation may cause initial temperature rise during the reaction process, to test the possibility of PS activation by heat or by VL irradiation, the effect of different temperatures on the PS activation was studied first for bacterial inactivation without light irradiation. As shown in Fig. 4(A), no bacterial inactivation is found when the temperature is 30 and 40 °C, indicating PS cannot be activated for bacterial inactivation when the temperature is below 40 °C without VL irradiation. With VL irradiation, the reaction temperature is maintained at about 30 °C. Therefore, in the VL/PS system, the observed PS activation should not be attributed to heat activation. This results further confirm the activation of PS by VL instead of heat. When the temperature is increased to 50 °C, the control experiments without PS addition show that about 1.5 log of viable cells are inactivated. In contrast, all the 7.0 log of cells can be completely inactivated within 60 min with PS addition. Therefore, the intrinsic bactericidal effect at 50 °C plays a minor role and the bacterial inactivation is mainly due to the effect of PS, which also suggests that 50 °C is the effective temperature for the activation of PS for bacterial inactivation if no light is used. This result is consistent with previous reports that 40–50 °C is the effective temperature for heat activation of PS for the degradation of organic pollutants (Ike et al., 2018). In addition, the •OH generation was monitored under different temperatures as shown in Fig. 4(B). The high PL intensity indicates a large amount of •OH is produced, which matches well with the high bacterial inactivation efficiency at 50 °C. Moreover, the radical generation was further verified by EPR spectroscopy using DMPO as spin-trapping reagent. As shown in Fig. 4(C), the obvious and gradually amplified signals of DMPO-•OH (1:2:2:1) are observed with increasing temperatures from 30 °C to 50 °C, which is in agreement with the result in Fig. 4(B). The corresponding PS decomposition rate was studied in Fig. 4(D). At 30 °C, negligible PS decomposition

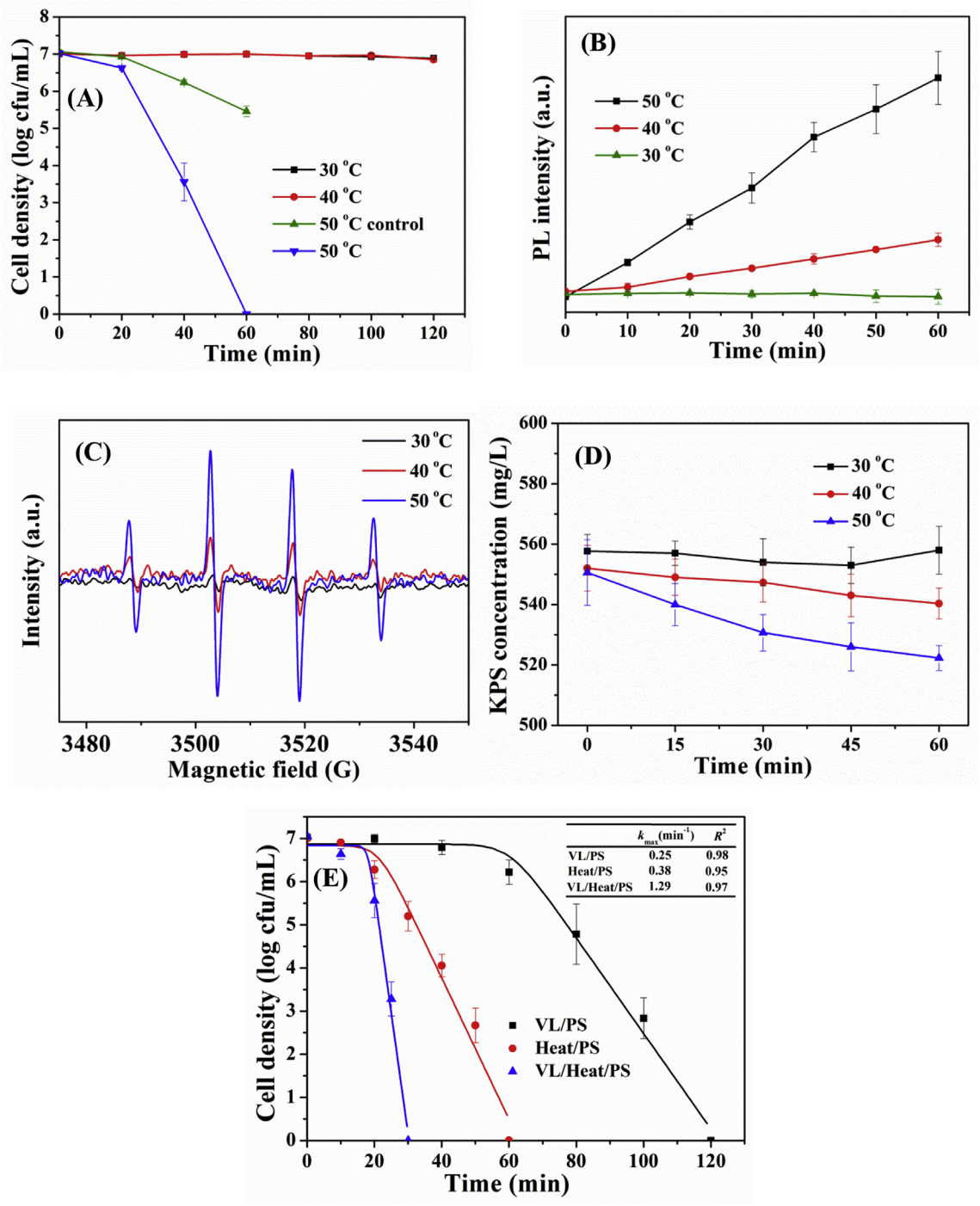

Fig. 4. (A) Bacterial inactivation efficiency by heat-activated PS under different temperatures; (B) Fluorescence intensity of coumarin solution (1 mM) with emission at 460 nm by heat-activated PS (Excitation at 332 nm); (C) EPR spectra of DMPO spin-trapping adducts for PS activation at different temperatures; (D) Corresponding PS decomposition rate at different temperatures; (E) Bacterial inactivation efficiency by VL/PS, heat/PS and VL/heat/PS with kinetic study by log-linear-shoulder model. Experimental conditions: cell density = 7 log cfu mL^{-1}; [PS] = 2 mM; $[pH]_0 = 6.0$; for VL/PS, $\lambda \geq 420$ nm, T = 30 °C; for heat/PS, T = 50 °C; for VL/heat/PS, $\lambda \geq 420$ nm, T = 50 °C.

was found. The decomposition rate increased gradually at higher temperature, following the first-order kinetics with rate constant k to be 3.67×10^{-4} and 8.78×10^{-4} min^{-1} for 40 °C and 50 °C, respectively. It was noted that although 40 °C is ineffective for bacterial inactivation by PS, a small amount of •OH can be detected, which may be attributed to the fact that the generated radicals are not enough to overcome the bacterial defending systems resulting in negligible cell death.

To study the possible synergistic effect of VL irradiation and heat activation of PS for disinfection, additional experiments were conducted under both VL irradiation and heating at 50 °C. As shown in Fig. 4(E), the bacterial inactivation efficiency was significantly promoted and 7 log of cells could be inactivated within 30 min. The inactivation kinetic was calculated according to the log-linear-shoulder model proposed by Geeraerd et al. (2005) (Equation (5)):

$$\log(N) = \log\left[\left(10^{\log(N_0)} - 10^{\log(N_{res})}\right) \times e^{-k_{max}t} \times \frac{e^{k_{max}S_l}}{1 + (e^{k_{max}S_l} - 1) \times e^{-k_{max}t}} + 10^{\log(N_{res})}\right] \quad (5)$$

where $N(0)$ is the initial cell destiny (cfu/mL), N_{res} is the residual cell density (cfu/mL), k_{max} is specific inactivation rate constant (min^{-1}) and S_l is the shoulder length (min). The k_{max} was calculated to be 0.25, 0.38 and 1.29 min^{-1} for bacterial inactivation by VL/PS, heat/PS and VL/heat/PS, respectively. The synergy factor could be then calculated according to the reference (Metheniti et al., 2018) (Equation (6)):

$$S(\%) = 100\frac{k_{combined} - \sum_i^n k_i}{k_{combined}} \quad (6)$$

where k_i is the rate constant of each individual process, while $k_{combined}$ is the rate constant of the combined process. The synergy factor was obtained to be 51.2%, suggesting the simultaneous use of VL and heat could result in synergistic effect rather than cumulative effect. The synergistic effect is important for practical application using solar light as the energy source, as sunlight irradiation will cause temperature rise which is expected to further accelerate the disinfection process.

3.2.2. Effect of pH, dissolved oxygen and inorganic ions

Bacterial inactivation efficiency in the VL/PS system was found to be highly dependent on pH, and lower pH can obtain higher inactivation performance (Fig. 5(A)). The control experiments with PS alone in dark at different pH were also conducted. No significant cell loss occurred in the pH range of 5.0–9.0, and only 1.0 log reduction of cells was found at pH 3.0 within 120 min, indicating the pH has no obvious inactivation effect on the cell viability (Fig. S4). *E. coli* is a representative of the large neutrophilic bacteria group, which grows optimally between pH 6.0 and 8.0. However, *E. coli* can also survive exposure to acidic pH (Lin et al., 1995). This acid tolerance response in *E. coli* involves acid-induced proteins that protect the cells from an acid shock (pH 3.0) (Heyde and Portalier, 1990; Rincon and Pulgarin, 2004a). The variation of pH was monitored as shown in Fig. 5(B). The pH remained stable in acidic condition (pH 3.0–5.0), and decreased slightly in neutral condition (pH 7.0). Notably, the pH decreased significantly from 9.0 to 6.8 in basic condition. This result matched well with previous studies that alkaline condition could provoke an accelerated PS decomposition, release H^+ and generate •OH radicals which is expected to increase the organic pollutant degradation activity (Furman et al., 2010). However, for bacterial inactivation in this study, acidic condition was found to favor the inactivation performance, and a significant decline of inactivation efficiency was observed with increasing pH values. This can be rationalized by considering the electrostatic adsorption of $S_2O_8^{2-}$ to bacterial cell surfaces. *E. coli* exists predominantly in its deprotonated form at pH 3.0–11.0, therefore almost all of the cells had a negative charge under such conditions, which would lead to the electrostatic repulsion between the deprotonated *E. coli* and $S_2O_8^{2-}$. A higher pH would further increase the electrostatic repulsion, resulting in declined bacterial inactivation efficiency. This result also indicates that the $S_2O_8^{2-}$ is really adsorbed onto the cell surface, and simultaneously activated by VL to produce $•SO_4^-$. The subsequent generating of •OH does not favor the disinfection efficiency, therefore the role of $•SO_4^-$ is more important than that of •OH radicals for bacterial inactivation, probably due to the fact that much longer half-life of the $•SO_4^-$ could enable it to penetrate through the cell membrane into the intracellular components.

The effect of dissolved O_2 in the VL/PS system was also studied. As shown in Fig. 5(C), total inactivation of 7 log *E. coli* cells was obtained within 120 min under both air equilibrium and O_2 purging, indicating the dissolved O_2 play a minor role in the disinfection process. In addition, with N_2 purging to create a complete anaerobic condition, the bacterial inactivation efficiency was only slightly decreased, further confirming that dissolved O_2 and its derived reactive oxygen radicals (i.e. •OH, $•O_2^-$) is not as important as $•SO_4^-$ for bacterial inactivation in this VL/PS system. Bicarbonate was the representative of inorganic carbon existed in natural water at the range of 0.1–50 mg/L, which can quench radicals to inhibit oxidation process (Wu et al., 2015). As shown in Fig. 5(D), a $NaHCO_3$ concentration of 1 mg/L exhibited similar inactivation efficiency with that of no $NaHCO_3$ addition; with further addition of $NaHCO_3$, the inactivation efficiency decreased significantly in the presence of 5 mg/L $NaHCO_3$ and almost completely inhibited when 20 mg L^{-1} of $NaHCO_3$ was used. The variation of pH was monitored during the reactions (Fig. 5(E)). It showed that the system pH was in the range of 6.2–7.8 with different concentrations of $NaHCO_3$ before the disinfection reactions. During the bacterial inactivation process, the pH remained stable due to the buffering effect of $NaHCO_3$. However, the basic conditions from $NaHCO_3$ would inhibit the bacterial inactivation process as discussed above (Fig. 5(A)). In addition, the bicarbonate could quench the $•SO_4^-$ to generate the $•CO_3^-$ with much lower redox potential (1.5 V) than that of $•SO_4^-$ (2.5–3.1 V) (Gao et al., 2016a; Miao et al., 2001). Therefore, both the basic pH and the quenching of $•SO_4^-$ would cause the detrimental effect to VL/PS system and greatly inhibit bacterial inactivation. The addition of other inorganic ions, including CH_3COO^-, SO_4^{2-}, NO_3^- and Cl^- could also retard the bacterial inactivation (Fig. 5(F)). The Cl^- was found to only slightly influence the bacterial inactivation. This could be due to the scavenging of $•SO_4^-$ by Cl^- to produce Cl• which then re-combined to generate molecular chlorine (Cl_2) (Rincon and Pulgarin, 2004a). The disinfection ability of Cl_2 is expected to compensate the loss of $•SO_4^-$, leading to the insignificant influence of Cl^-.

3.3. Bacterial inactivation process and mechanism

To understand the bacterial inactivation mechanism, the activities of several intracellular antioxidant enzymes were monitored respectively during the bacterial inactivation process. Superoxide dismutase (SOD) is a well-known antioxidant enzyme that catalyzes the decomposition of $•O_2^-$ to H_2O_2, while catalase (CAT) can further catalyze the decomposition of H_2O_2 to water and oxygen (Wang et al., 2013). Therefore, a higher SOD and CAT activity indicates the cells are encountering a more severe oxidative stress from the environment. The SOD and CAT activities were determined during the bacterial inactivation process. As shown in Fig. 6(A) and (B), in the initial 2 h, both SOD and CAT activity increased rapidly with irradiation time, which indicates there is a large amount of oxidative radicals attacking the bacteria at the beginning of the inactivation process, with the bacterial defense system displaying a higher SOD and CAT activity to protect the bacterial cells. This observation matches well with the results of Fig. 1(A) which showed that the disinfection efficiency increased very slowly within the initial 2 h because these antioxidative enzymes protected the *E. coli*. After 2 h, both SOD and CAT activity gradually decreased as the bacterial inactivation process progressed. This result can be reasonably explained by the rapid increase of the disinfection efficiency after 2 h (Fig. 1(A)). It is because that when the amount of produced radicals exceeded the protection ability of the bacterial defense system, *E. coli* cells was severely damaged, and the activities of both enzymes decreased again. In

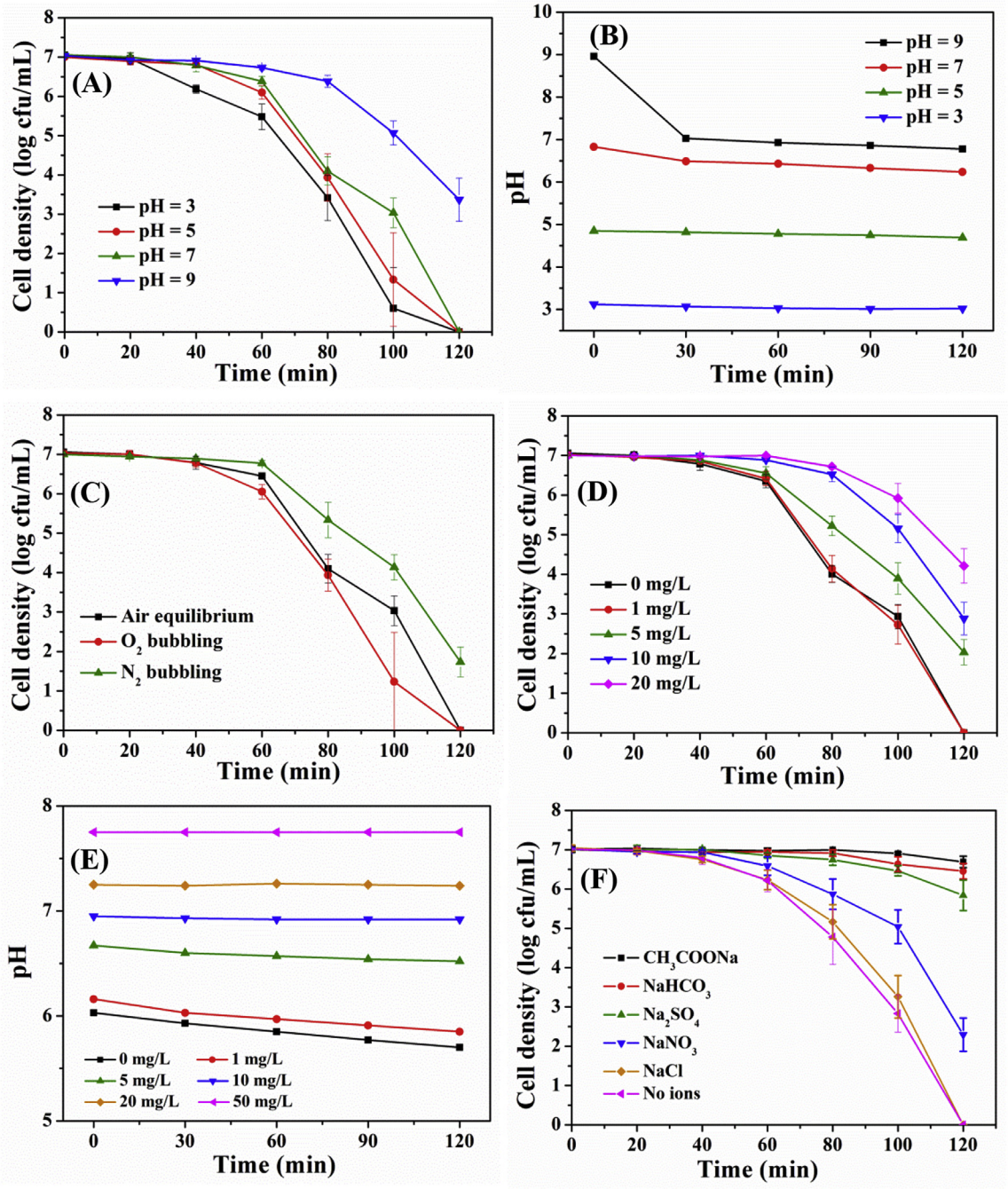

Fig. 5. Bacterial inactivation efficiency in the VL/PS system: (A) Effect of different initial pH; (B) Variation of pH during the reactions with different initial pH; (C) Effect of different aeration conditions; (D) Effect of 0–20 mg/L bicarbonate; (E) Variation of pH during the reactions with bicarbonate; (F) Effects of different inorganic anions (0.1 M) on the bacterial inactivation efficiency in the VL/PS system. Experimental conditions: cell density = 7 log cfu mL^{-1}; [PS] = 2 mM; $\lambda \geq 420$ nm; T = 30 °C; $[pH]_0 = 6.0$.

contrast, negligible SOD and CAT activity was observed under light control (without PS) and dark control (without VL irradiation) conditions. This evidence further confirms the radical-induced oxidative inactivation of bacterial cells in the VL/PS system. Both VL and PS are the prerequisites for the bacterial inactivation.

To further understand the intracellular oxidative stress, the intracellular ROS level was also tested using a DCFH-DA probe, which can be hydrolyzed to non-fluorescent dichlorofluorescein (DCFH) by esterase in the cells and can further be oxidized to produce the fluorescent dichlorofluorescein (DCF) by cellular ROS. As shown in Fig. 6(C), the intracellular ROSs level was found to increase steadily with the reaction time in the VL/PS system, while no intracellular ROSs promotion was found under light and dark controls, suggesting the cells are encountering ROSs attacking at all the time in the VL/PS process. When the accumulated ROSs overwhelmed the defense system, the cells were gradually damaged to death. The bacterial inactivation process was further observed by SEM technologies (Fig. 7). It showed that the untreated *E. coli* cell exhibits intact and smooth outer membrane. After VL irradiation for 30 min, the outer membrane of the cell wall started to wrinkle and become rough, suggesting the bacteria suffered from external oxidative stress. With the time going to 60–90 min, the cell surface

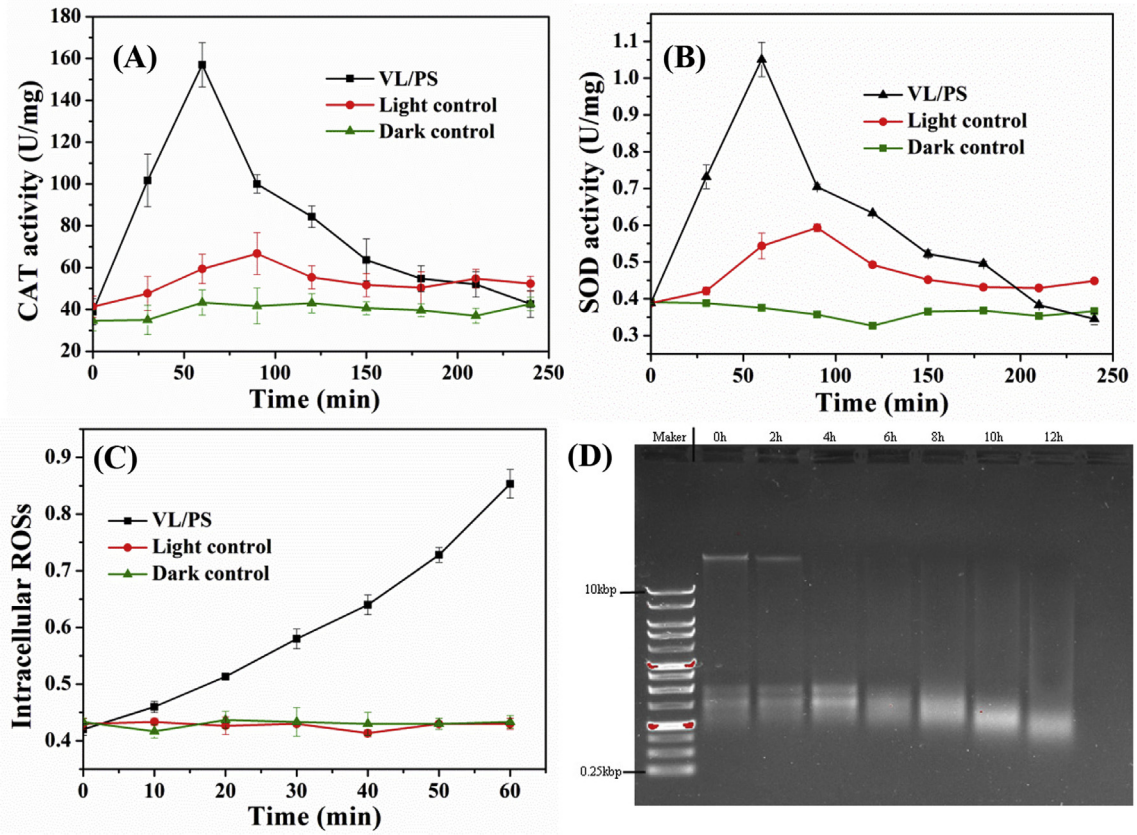

Fig. 6. (A) CAT activity; (B) SOD activity; (C) Intracellular ROSs levels and (D) destruction of bacterial genomic DNA extracted from harvested cells during treatment in the VL/PS system. Experimental conditions: cell density = 8 log cfu mL^{-1}; [PS] = 2 mM; $\lambda \geq 420$ nm; T = 30 °C; $[pH]_0 = 6.0$.

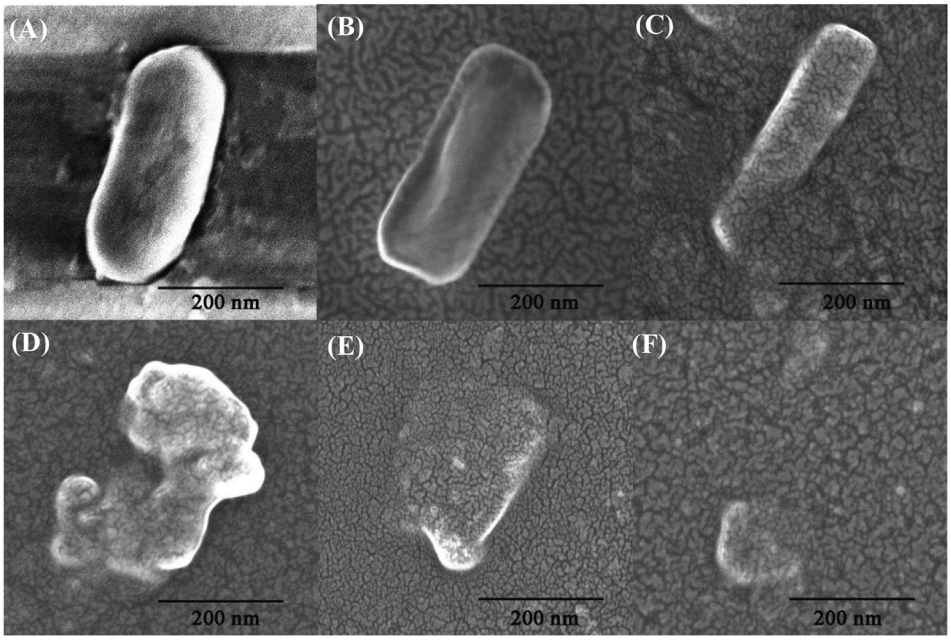

Fig. 7. SEM images of *E. coli* cell treated by the VL/PS system with different irradiation time: (A) 0 min; (B); 30 min; (C) 60 min; (D) 90 min; (E) 120 min; (F) 150 min. Experimental conditions: cell density = 7 log cfu mL^{-1}; [PS] = 2 mM; $\lambda \geq 420$ nm; T = 30 °C; $[pH]_0 = 6.0$.

become rougher, and lots of holes were observed on the outer membrane. Finally, after 120–150 min of VL irradiation, the cell structure was completely ruptured, leaving only small pieces of cell debris. Therefore, the cell destruction process was confirmed from outer membrane to intracellular components. After the penetration of cell membrane, the oxidative radicals can subsequently injure

the cells by reacting with various biomolecules, such as cytoplasmic protein and genome (Sun et al., 2014). As shown in Fig. 6(D), the destruction of genomic DNA was observed as the fluorescent intensity of the DNA bands started to fade with VL irradiation and almost disappeared with time prolonged to 12 h. Only severe damage to chromosomal DNA is lethal to the cells. Otherwise, cells in a viable but non-culturable state may still revive to cause the health risks in water (Zhang et al., 2015). Therefore, the new disinfection method of VL/PS can not only inactivate the bacterial cells, but also can kill the cells leaving no regrowth ability.

Based on the above results, the bacterial inactivation mechanism in the VL/PS system is illustrated as shown in Fig. 8. At first, the $S_2O_8^{2-}$ is activated by VL to produce $\bullet SO_4^-$ in solution, which then partially transforms to $\bullet O_2^-$ and •OH. The $\bullet SO_4^-$ has much longer life time as well as stronger oxidation power than that of $\bullet O_2^-$ and •OH, causing severe damage to the cell membrane. Subsequently, the radical species penetrated through the membrane and high levels of intracellular antioxidant enzyme are induced to annihilate the oxidative stress of ROSs. Finally, the defense systems are destroyed with increasing amount of ROSs, leading to carbonylation of cytoplasmic protein and damage to genomic DNA. It is noted that previous studies have reported the activation of PS by various catalysts combined with VL irradiation (Tang et al., 2019; Yang et al., 2019). However, these studies have only focused on the effect of catalysts, and ignored the intrinsic effect of PS under VL irradiation, probably due to the low PS concentration and the recalcitrant organic pollutants. To the best of our knowledge, this is the first report about the PS activation by VL for bacterial inactivation without catalysts. The bacterial inactivation efficiency is closely related to PS concentration (Fig. 1(B)), suggesting sufficient PS concentration is crucial in the VL/PS system. Gao et al. (2017) has reported a catalyst-free activation of PS by VL for dye (i.e. RhB, Eosin Y) degradation, in which the dyes were functioned like photosensitizers to "catalyze" the reaction by exciting electrons to activate PS, instead of direct activation by VL in this study. In a recent study, Pan et al. (2018) has reported a very low efficiency (~20%) for the benzophenone-3 degradation by PS under VL ($\lambda = 420$ nm). In our study, the bacterial cells can absorb visible photons, which has been well proved in previous studies (Vermeulen et al., 2008; Kielbassa et al., 1997; Chen et al., 2018). Therefore, besides the activation of PS by VL, the bacterial cells may be able to further accelerate the PS activation process by transferring the visible photon energy to activate PS, similar to the "photosensitization" mechanism. Therefore, it is expected that the PS with sufficient concentration can be activated by VL for dye degradation and bacterial inactivation, but may not for other organic contaminant which cannot absorb visible light, unless an even high PS concentration is used.

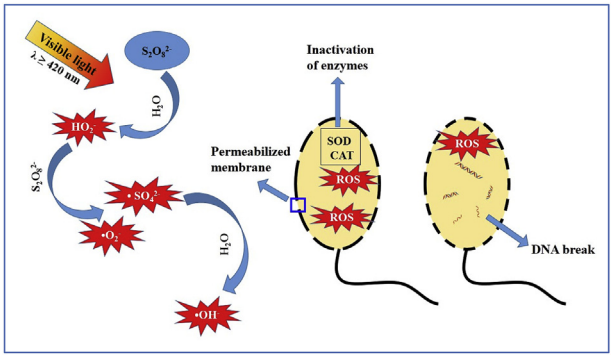

Fig. 8. Schematic diagram of the bacterial inactivation mechanism in the VL/PS system.

3.4. Universality of the VL/PS system for water disinfection

To further investigate the universality and potential application of the VL/PS system in water disinfection, other pathogenic bacteria including *Staphylococcus aureus* (*S. aureus*) and *Pseudomonas aeruginosa* (*P. aeruginosa*) were also used to test the inactivation efficiency. *S. aureus* is a Gram-positive bacterium and a common cause of skin infections including abscesses, respiratory infections such as sinusitis, and food poisoning. As shown in Fig. 9(A), 7-log of *S. aureus* could be also totally inactivated within 200 min under VL irradiation with 2 mM PS. In contrast, no bacterial inactivation was found under dark and light conditions. *P. aeruginosa* is a Gram-negative bacterium and is a multidrug resistant pathogen associated with hospital-acquired infections (HAI) (Peleg and Hooper, 2010). Similarly, VL/PS system also shows high inactivation efficiency for the *P. aeruginosa*, and 7-log of cells could be completely inactivated within 140 min (Fig. 9(B)). It is noted that the inactivation efficiency of three tested strains follows the order of: *E. coli* > *P. aeruginosa* > *S. aureus*. This can be explained by considering the different cell structure of Gram-positive and Gram-negative bacterium. The Gram-positive bacterium has a much thicker cell wall constructed by peptidoglycan layer (20–80 nm vs. 10 nm in Gram-negative bacterium), which make it to be more

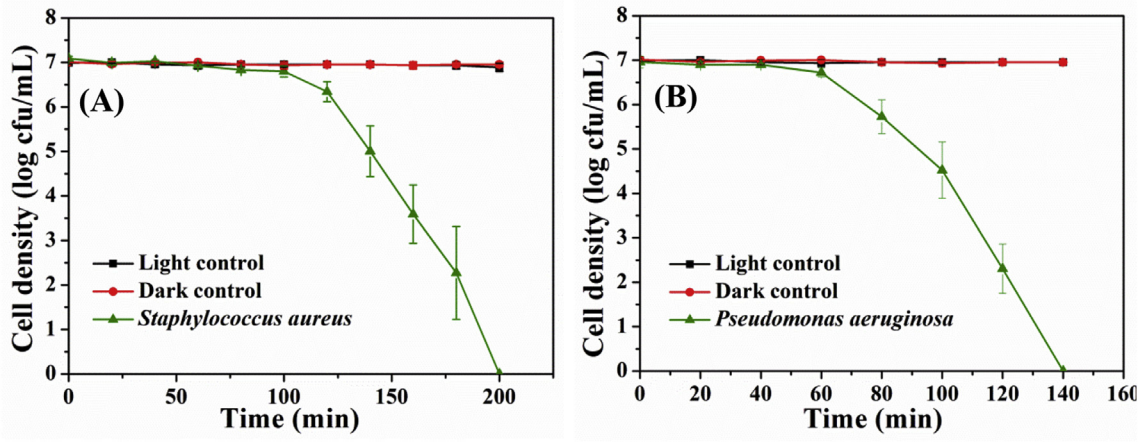

Fig. 9. Bacterial inactivation efficiency for (A) *S. aureus* and (B) *P. aeruginosa* by the VL/PS system. Experimental conditions: cell density = 7 log cfu mL^{-1}; [PS] = 2 mM; $\lambda \geq 420$ nm; T = 30 °C; $[pH]_0 = 6.0$.

resistant to ROSs attacking (Chen et al., 2013). Therefore, *S. aureus* shows the lowest inactivation efficiency. In addition, due to the intrinsic multidrug resistant mechanism, *P. aeruginosa* is more resistant to adverse environment changes compared with *E. coli*, and therefore it shows lower inactivation efficiency than that of *E. coli*. Nevertheless, the VL/PS system is applicable to inactivate both Gram-positive, Gram-negative and multidrug resistant pathogens, showing great potential to be used for universal authentic water disinfection. It is noted that during the process, the consumption of PS will cause the increase of sulfate anions. According to the guidelines for drinking water quality by the World Health Organization (WHO), the limit above which sulfate anions affect the taste of drinking water is 250 mg/L (Ioannidi et al., 2018). The PS consumption after the complete bacterial inactivation in the VL/PS system is ~43.6 mg/L (Fig. 2(D)), corresponding to sulfate anions of ~31 mg/L. Therefore, the increased concentration of sulfate anions is far less than the standard value (250 mg/L), and should not have obvious impact on water quality.

The demands for "green" and sustainable development calls for new technologies without the use of a catalyst for environmental remediation using sunlight as the energy source, in order to overcome the high-cost and recycling problems of artificial catalysts. Previous studies have confirmed that UV light which accounts for ~5% of sunlight spectrum can be used for PS activation for organic pollutant degradation and bacterial inactivation, but ignored the intrinsic effect of VL which accounts for ~48% of sunlight spectrum. This study indicates PS can also be activated by VL for water disinfection, thus the sunlight usage can be improved from ~5% to ~53%. Although the VL response is only extended to 420 nm at this stage, it is expected that this work will open an avenue for on-going research efforts to further enlarge the light response, eventually achieving the ultimate goal of catalyst-free environmental remediation using inexhaustible solar energy.

4. Conclusions

In this study, a new catalyst-free visible light driven PS activation method was developed for water disinfection. Total inactivation of 6-log *E. coli* cells within 40 min and 7 log within 120 min could be achieved under VL irradiation in the presence of 2 mM PS solution. Increasing the PS concentration in the range of 2–4 mM could further promote the bacterial inactivation efficiency, but no heat activation of PS effect was found during the VL/PS process. The major responsive wavelength was determined to be 420 nm by monochromic light irradiation. The acidic pH was benefit for the VL/PS-triggered bacterial inactivation, while bicarbonate inhibited the *E. coli* inactivation at the range of 0.1–20 mg L^{-1} and dissolved O_2 plays minor roles in the inactivation efficiency. Mechanism study further indicates the main reactive species are $\bullet SO_4^-$, $\bullet O_2^-$ and $\bullet OH$, in which $\bullet SO_4^-$ plays the most important role. The bacterial inactivation process was identified to begin from outer membrane to intracellular components. The $S_2O_8^{2-}$ was activated by VL to produce oxidative radicals which cause the damage of cell membrane. Subsequently, several antioxidant enzymes, such as CAT and SOD were induced, followed by damage to the genomic DNA, leading to the cell death. Besides *E. coli*, other typical pathogenic bacteria including *S. aureus* and *P. aeruginosa* could also be effectively inactivated by this VL/PS system. This study not only provides a novel cost-effective method for PS-activated water disinfection without the use of a catalyst, but also provides new insights into understanding the bacterial inactivation mechanisms. The catalyst-free VL/PS system is also expected to find applications in other environmental-related purification.

Acknowledgements

This work was supported by the National Natural Science Foundation of China (No. 21607028, 41425015 and 41573086), the Research Grant Council of Hong Kong SAR Government (GRF14100115), Science and Technology Project of Guangdong Province, China (2017A050506049), Local Innovative and Research Teams Project of Guangdong Pearl River Talents Program (2017BT01Z032), Innovation Team Project of Guangdong Provincial Department of Education (2017KCXTD012) and Leading Scientific, Technical and Innovation Talents of Guangdong special support program (2016TX03Z094).

Appendix A. Supplementary data

Supplementary data related to this article can be found at https://doi.org/10.1016/j.watres.2019.03.071.

References

Ahmad, M., Teel, A.L., Watts, R.J., 2013. Mechanism of persulfate activation by phenols. Environ. Sci. Technol. 47, 5864–5871.
An, D., Westerhoff, P., Zheng, M.X., Wu, M.Y., Yang, Y., Chiu, C.A., 2015. UV-activated persulfate oxidation and regeneration of NOM-Saturated granular activated carbon. Water Res. 73, 304–310.
Anastasi, E.M., Wohlsen, T.D., Stratton, H.M., Katouli, M., 2013. Survival of *Escherichia coli* in two sewage treatment plants using UV irradiation and chlorination for disinfection. Water Res. 47, 6670–6679.
Antoniou, M.G., de la Cruz, A.A., Dionysiou, D.D., 2010. Degradation of microcystin-LR using sulfate radicals generated through photolysis, thermolysis and e^- transfer mechanisms. Appl. Catal. B Environ. 96, 290–298.
Babuponnusami, A., Muthukumar, K., 2012. Advanced oxidation of phenol: a comparison between Fenton, electro-Fenton, sono-electro-Fenton and photo-electro-Fenton processes. Chem. Eng. J. 183, 1–9.
Brillas, E., Sires, I., Oturan, M.A., 2009. Electro-Fenton process and related electrochemical technologies based on Fenton's reaction chemistry. Chem. Rev. 109, 6570–6631.
Catley-Carlson, M., 2017. Water supply: the emptying well. Nature 542, 412–413.
Chen, X., Yin, H., Li, G., Wang, W., Wong, P.K., Zhao, H., An, T., 2018. Antibiotic-resistance gene transfer in antibiotic-resistance bacteria under different light irradiation: implications from oxidative stress and gene expression. Water Res. 149, 282–291.
Chen, Y.M., Ng, T.W., Lu, A.H., Li, Y., Yip, H.Y., An, T.C., Li, G.Y., Zhao, H.J., Gao, M.H., Wong, P.K., 2013. Comparative study of visible-light-driven photocatalytic inactivation of two different wastewater bacteria by natural sphalerite. Chem. Eng. J. 234, 43–48.
Dalrymple, O.K., Stefanakos, E., Trotz, M.A., Goswami, D.Y., 2010. A review of the mechanisms and modeling of photocatalytic disinfection. Appl. Catal. B Environ. 98, 27–38.
De Luca, A., He, X.X., Dionysiou, D.D., Dantas, R.F., Esplugas, S., 2017. Effects of bromide on the degradation of organic contaminants with UV and Fe^{2+} activated persulfate. Chem. Eng. J. 318, 206–213.
Du, X.D., Zhang, Y.Q., Hussain, I., Huang, S.B., Huang, W.L., 2017. Insight into reactive oxygen species in persulfate activation with copper oxide: activated persulfate and trace radicals. Chem. Eng. J. 313, 1023–1032.
Duan, X.G., Sun, H.Q., Kang, J., Wang, Y.X., Indrawirawan, S., Wang, S.B., 2015. Insights into heterogeneous catalysis of persulfate activation on dimensional-structured nanocarbons. ACS Catal. 5, 4629–4636.
Duan, X.G., Ao, Z.M., Zhou, L., Sun, H.Q., Wang, G.X., Wang, S.B., 2016a. Occurrence of radical and nonradical pathways from carbocatalysts for aqueous and nonaqueous catalytic oxidation. Appl. Catal. B Environ. 188, 98–105.
Duan, X.G., Su, C., Zhou, L., Sun, H.Q., Suvorova, A., Odedairo, T., Zhu, Z.H., Shao, Z.P., Wang, S.B., 2016b. Surface controlled generation of reactive radicals from persulfate by carbocatalysis on nanodiamonds. Appl. Catal. B Environ. 194, 7–15.
Fang, G.D., Gao, J., Dionysiou, D.D., Liu, C., Zhou, D.M., 2013. Activation of persulfate by quinones: free radical reactions and implication for the degradation of PCBs. Environ. Sci. Technol. 47, 4605–4611.
Farhat, A., Keller, J., Tait, S., Radjenovic, J., 2015. Removal of persistent organic contaminants by electrochemically activated sulfate. Environ. Sci. Technol. 49, 14326–14333.
Feng, M., Qu, R., Zhang, X., Sun, P., Sui, Y., Wang, L., Wang, Z., 2015. Degradation of flumequine in aqueous solution by persulfate activated with common methods and polyhydroquinone-coated magnetite/multi-walled carbon nanotubes catalysts. Water Res. 85, 1–10.
Furman, O.S., Teel, A.L., Watts, R.J., 2010. Mechanism of base activation of persulfate. Environ. Sci. Technol. 44, 6423–6428.
Gao, H.P., Chen, J.B., Zhang, Y.L., Zhou, X.F., 2016a. Sulfate radicals induced degradation of Triclosan in thermally activated persulfate system. Chem. Eng. J. 306, 522–530.

Gao, Y.W., Li, Y.X., Yao, L.Y., Li, S.M., Liu, J., Zhang, H., 2017. Catalyst-free activation of peroxides under visible LED light irradiation through photoexcitation pathway. J. Hazard Mater. 329, 272–279.
Gao, Y.W., Zhang, Z.Y., Li, S.M., Liu, J., Yao, L.Y., Li, Y.X., Zhang, H., 2016b. Insights into the mechanism of heterogeneous activation of persulfate with a clay/iron-based catalyst under visible LED light irradiation. Appl. Catal. B Environ. 185, 22–30.
Geeraerd, A.H., Valdramidis, V., Van Impe, J.F., 2005. GInaFiT, a freeware tool to assess non-log-linear microbial survivor curves. Int. J. Food Microbiol. 102, 95–105.
Giannakis, S., Le, T.T.M., Entenza, J.M., Pulgarin, C., 2018. Solar photo-Fenton disinfection of 11 antibiotic-resistant bacteria (ARB) and elimination of representative AR genes. Evidence that antibiotic resistance does not imply resistance to oxidative treatment. Water Res. 143, 334–345.
Guan, H.M., Zhu, L.H., Zhou, H.H., Tang, H.Q., 2008. Rapid probing of photocatalytic activity on titania-based self-cleaning materials using 7-hydroxycoumarin fluorescent probe. Anal. Chim. Acta 608, 73–78.
Guan, Y.H., Ma, J., Li, X.C., Fang, J.Y., Chen, L.W., 2011. Influence of pH on the formation of sulfate and hydroxyl radicals in the UV/peroxymonosulfate system. Environ. Sci. Technol. 45, 9308–9314.
Guo, S., Yang, Z.X., Wen, Z.P., Fida, H., Zhang, G.K., Chen, J.Y., 2018. Reutilization of iron sludge as heterogeneous Fenton catalyst for the degradation of Rhodamine B: role of sulfur and mesoporous structure. J. Colloid Interface Sci. 532, 441–448.
Haaken, D., Schmalz, V., Dittmar, T., Worch, E., 2013. Limits of UV disinfection: UV/electrolysis hybrid technology as a promising alternative for direct reuse of biologically treated wastewater. J. Water Supply Res. Technol. - Aqua 62, 442–451.
Heyde, M., Portalier, R., 1990. Acid shock proteins of *Escherichia coli*. FEMS Microbiol. Lett. 57, 19–26.
Ike, I.A., Orbell, J.D., Duke, M., 2018. Activation of persulfate at waste heat temperatures for humic acid degradation. ACS Sustain. Chem. Eng. 6, 4345–4353.
Ioannidi, A., Frontistis, Z., Mantzavinos, D., 2018. Destruction of propyl paraben by persulfate activated with UV-A light emitting diodes. J. Environ. Chem. Eng. 6, 2992–2997.
Ishibashi, K., Fujishima, A., Watanabe, T., Hashimoto, K., 2000. Detection of active oxidative species in TiO_2 photocatalysis using the fluorescence technique. Electrochem. Commun. 2, 207–210.
Kang, J., Duan, X.G., Zhou, L., Sun, H.Q., Tade, M.O., Wang, S.B., 2016. Carbocatalytic activation of persulfate for removal of antibiotics in water solutions. Chem. Eng. J. 288, 399–405.
Khan, J.A., He, X.X., Shah, N.S., Sayed, M., Khan, H.M., Dionysiou, D.D., 2017. Degradation kinetics and mechanism of desethyl-atrazine and desisopropyl-atrazine in water with •OH and $•SO_4^-$- based-AOPs. Chem. Eng. J. 325, 485–494.
Kielbassa, C., Roza, L., Epe, B., 1997. Wavelength dependence of oxidative DNA damage induced by UV and visible light. Carcinogenesis 18, 811–816.
Lee, H., Lee, H.J., Jeong, J., Lee, J., Park, N.B., Lee, C., 2015. Activation of persulfates by carbon nanotubes: oxidation of organic compounds by nonradical mechanism. Chem. Eng. J. 266, 28–33.
Liang, C.J., Wang, Z.S., Bruell, C.J., 2007. Influence of pH on persulfate oxidation of TCE at ambient temperatures. Chemosphere 66, 106–113.
Liang, C.J., Huang, C.F., Mohanty, N., Kurakalva, R.M., 2008. A rapid spectrophotometric determination of persulfate anion in ISCO. Chemosphere 73, 1540–1543.
Liang, H.W., Sun, H.Q., Patel, A., Shukla, P., Zhu, Z.H., Wang, S.B., 2012. Excellent performance of mesoporous Co_3O_4/MnO_2 nanoparticles in heterogeneous activation of peroxymonosulfate for phenol degradation in aqueous solutions. Appl. Catal. B Environ. 127, 330–335.
Lin, J., Lee, I.S., Frey, J., Slonczewski, J.L., Foster, J.W., 1995. Comparative analysis of extreme acid survival in *Salmonella typhimurium, Shigella flexneri*, and *Escherichia coli*. J. Bacteriol. 177, 4097–4104.
Liu, C.S., Higgins, C.P., Wang, F., Shih, K., 2012. Effect of temperature on oxidative transformation of perfluorooctanoic acid (PFOA) by persulfate activation in water. Separ. Purif. Technol. 91, 46–51.
Liu, H.Z., Bruton, T.A., Doyle, F.M., Sedlak, D.L., 2014. *In situ* chemical oxidation of contaminated groundwater by persulfate: decomposition by Fe(III)- and Mn(IV)-containing oxides and aquifer materials. Environ. Sci. Technol. 48, 10330–10336.
Liu, Y.Q., He, X.X., Fu, Y.S., Dionysiou, D.D., 2016. Kinetics and mechanism investigation on the destruction of oxytetracycline by UV-254 nm activation of persulfate. J. Hazard Mater. 305, 229–239.
Liu, Z., Zhao, C., Wang, P., Zheng, H.L., Sun, Y.J., Dionysiou, D.D., 2018. Removal of carbamazepine in water by electro-activated carbon fiber-peroxydisulfate: comparison, optimization, recycle, and mechanism study. Chem. Eng. J. 343, 28–36.
Lu, J.H., Yang, P.Z., Dong, W., Ji, Y.F., Huang, Q.G., 2018. Enhanced formation of chlorinated disinfection byproducts in the UV/chlorine process in the presence of benzophenone-4. Chem. Eng. J. 351, 304–311.
Luo, M.X., Lv, L.P., Deng, G.W., Yao, W., Ruan, Y., Li, X.X., Xu, A.H., 2014. The mechanism of bound hydroxyl radical formation and degradation pathway of Acid Orange II in Fenton-like Co^{2+}-HCO_3- system. Appl. Catal. Gen. 469, 198–205.
Metheniti, M.E., Frontistis, Z., Ribeiro, R.S., Silva, A.M.T., Faria, J.L., Gomes, H.T., Mantzavinos, D., 2018. Degradation of propyl paraben by activated persulfate using iron-containing magnetic carbon xerogels: investigation of water matrix and process synergy effects. Environ. Sci. Pollut. Res. 25, 34801–34810.
Miao, J.L., Wang, W.F., Pan, J.X., Lu, C.Y., Li, R.Q., Yao, S.D., 2001. The scavenging reactions of nitrogen dioxide radical and carbonate radical by tea polyphenol derivatives: a pulse radiolysis study. Radiat. Phys. Chem. 60, 163–168.
Michael-Kordatou, I., Iacovou, M., Frontistis, Z., Hapeshi, E., Dionysiou, D.D., Fatta-Kassinos, D., 2015. Erythromycin oxidation and ERY-resistant *Escherichia coli* inactivation in urban wastewater by sulfate radical-based oxidation process under UV-C irradiation. Water Res. 85, 346–358.
Montgomery, M.A., Elimelech, M., 2007. Water and sanitation in developing countries: including health in the equation. Environ. Sci. Technol. 41, 17–24.
Ng, T.W., An, T.C., Li, G.Y., Ho, W.K., Yip, H.Y., Zhao, H.J., Wong, P.K., 2015. The role and synergistic effect of the light irradiation and H_2O_2 in photocatalytic inactivation of *Escherichia coli*. J. Photochem. Photobiol. B Biol. 149, 164–171.
Pan, X.X., Yan, L.Q., Qu, R.J., Wang, Z.Y., 2018. Degradation of the UV-filter benzophenone-3 in aqueous solution using persulfate activated by heat, metal ions and light. Chemosphere 196, 95–104.
Parker, K.M., Zeng, T., Harkness, J., Vengosh, A., Mitch, W.A., 2014. Enhanced formation of disinfection byproducts in shale gas wastewater-impacted drinking water supplies. Environ. Sci. Technol. 48, 11161–11169.
Peleg, A.Y., Hooper, D.C., 2010. Hospital-acquired infections due to Gram-negative bacteria. N. Engl. J. Med. 362, 1804–1813.
Qi, C.D., Liu, X.T., Lin, C.Y., Zhang, H.J., Li, X., Ma, J., 2017. Activation of peroxymonosulfate by microwave irradiation for degradation of organic contaminants. Chem. Eng. J. 315, 201–209.
Rincon, A.G., Pulgarin, C., 2004a. Effect of pH, inorganic ions, organic matter and H_2O_2 on *E. coli* K12 photocatalytic inactivation by TiO_2 - implications in solar water disinfection. Appl. Catal. B Environ. 51, 283–302.
Rincon, A.G., Pulgarin, C., 2004b. Bactericidal action of illuminated TiO_2 on pure *Escherichia coli* and natural bacterial consortia: post-irradiation events in the dark and assessment of the effective disinfection time. Appl. Catal. B Environ. 49, 99–112.
Rizzo, L., Fiorentino, A., Anselmo, A., 2013. Advanced treatment of urban wastewater by UV radiation: effect on antibiotics and antibiotic-resistant *E. coli* strains. Chemosphere 92, 171–176.
Sichel, C., Blanco, J., Malato, S., Fernandez-Ibanez, P., 2007. Effects of experimental conditions on *E. coli* survival during solar photocatalytic water disinfection. J. Photochem. Photobiol. A Chem. 189, 239–246.
Sun, H.W., Li, G.Y., Nie, X., Shi, H.X., Wong, P.K., Zhao, H.J., An, T.C., 2014. Systematic approach to in-depth understanding of photoelectrocatalytic bacterial inactivation mechanisms by tracking the decomposed building blocks. Environ. Sci. Technol. 48, 9412–9419.
Tang, H., Dai, Z., Xie, X.D., Wen, Z.P., Chen, R., 2019. Promotion of peroxydisulfate activation over $Cu_{0.84}Bi_{2.08}O_4$ for visible light induced photodegradation of ciprofloxacin in water matrix. Chem. Eng. J. 356, 472–482.
Vermeulen, N., Keeler, W.J., Nandakumar, K., Leung, K.T., 2008. The bactericidal effect of ultraviolet and visible light on *Escherichia coli*. Biotechnol. Bioeng. 99, 550–556.
Waldemer, R.H., Tratnyek, P.G., Johnson, R.L., Nurmi, J.T., 2007. Oxidation of chlorinated ethenes by heat-activated persulfate: kinetics and products. Environ. Sci. Technol. 41, 1010–1015.
Wang, J.L., Wang, S.Z., 2018. Activation of persulfate (PS) and peroxymonosulfate (PMS) and application for the degradation of emerging contaminants. Chem. Eng. J. 334, 1502–1517.
Wang, W.J., Huang, G.C., Yu, J.C., Wong, P.K., 2015. Advances in photocatalytic disinfection of bacteria: development of photocatalysts and mechanisms. J. Environ. Sci. 34, 232–247.
Wang, W.J., Zhang, L.Z., An, T.C., Li, G.Y., Yip, H.Y., Wong, P.K., 2011. Comparative study of visible-light-driven photocatalytic mechanisms of dye decolorization and bacterial disinfection by B-Ni-codoped TiO_2 microspheres: the role of different reactive species. Appl. Catal. B Environ. 108, 108–116.
Wang, W.J., Li, G.Y., Xia, D.H., An, T.C., Zhao, H.J., Wong, P.K., 2017. Photocatalytic nanomaterials for solar-driven bacterial inactivation: recent progress and challenges. Environ. Sci.: Nano 4, 782–799.
Wang, W.J., Li, G.Y., An, T.C., Chan, D.K.L., Yu, J.C., Wong, P.K., 2018. Photocatalytic hydrogen evolution and bacterial inactivation utilizing sonochemical-synthesized g-C_3N_4/red phosphorus hybrid nanosheets as a wide-spectral-responsive photocatalyst: the role of type I band alignment. Appl. Catal. B Environ. 238, 126–135.
Wang, W.J., Yu, Y., An, T.C., Li, G.Y., Yip, H.Y., Yu, J.C., et al., 2012. Visible-light-driven photocatalytic inactivation of *E. coli* K-12 by bismuth vanadate nanotubes: bactericidal performance and mechanism. Environ. Sci. Technol. 46, 4599–4606.
Wang, W.J., Ng, T.W., Ho, W.K., Huang, J.H., Liang, S.J., An, T.C., Li, G.Y., Yu, J.C., Wong, P.K., 2013. $CdIn_2S_4$ microsphere as an efficient visible-light-driven photocatalyst for bacterial inactivation: synthesis, characterizations and photocatalytic inactivation mechanisms. Appl. Catal. B Environ. 129, 482–490.
Wei, Z.S., Villamena, F.A., Weavers, L.K., 2017. Kinetics and mechanism of ultrasonic activation of persulfate: an in situ EPR spin trapping study. Environ. Sci. Technol. 51, 3410–3417.
Wu, Y.L., Bianco, A., Brigante, M., Dong, W.B., de Sainte-Claire, P., Hanna, K., Mailhot, G., 2015. Sulfate radical photogeneration using Fe-EDDS: influence of critical parameters and naturally occurring scavengers. Environ. Sci. Technol. 49, 14343–14349.
Xia, D.H., Li, Y., Huang, G.C., Yin, R., An, T.C., Li, G.Y., Zhao, H.J., Lu, A.H., Wong, P.K., 2017. Activation of persulfates by natural magnetic pyrrhotite for water disinfection: efficiency, mechanisms, and stability. Water Res. 112, 236–247.
Yang, L., Xu, L., Bai, X., Jin, P., 2019. Enhanced visible-light activation of persulfate by

Ti^{3+} self-doped TiO_2/graphene nanocomposite for the rapid and efficient degradation of micropollutants in water. J. Hazard Mater. 365, 107–117.
Zhang, S.H., Ye, C.S., Lin, H.R., Lv, L., Yu, X., 2015. UV disinfection induces a VBNC state in *Escherichia coli* and *Pseudomonas aeruginosa*. Environ. Sci. Technol. 49, 1721–1728.
Zhao, Q.X., Mao, Q.M., Zhou, Y.Y., Wei, J.H., Liu, X.C., Yang, J.Y., Luo, L., Zhang, J.C., Chen, H., Chen, H.B., Tang, L., 2017. Metal-free carbon materials-catalyzed sulfate radical-based advanced oxidation processes: a review on heterogeneous catalysts and applications. Chemosphere 189, 224–238.
Zhao, Y.S., Sun, C., Sun, J.Q., Zhou, R., 2015. Kinetic modeling and efficiency of sulfate radical-based oxidation to remove p-nitroaniline from wastewater by persulfate/Fe_3O_4 nanoparticles process. Separ. Purif. Technol. 142, 182–188.
Zhu, C.Y., Fang, G.D., Dionysiou, D.D., Liu, C., Gao, J., Qin, W.X., Zhou, D.M., 2016. Efficient transformation of DDTs with persulfate activation by zero-valent iron nanoparticles: a mechanistic study. J. Hazard Mater. 316, 232–241.
Zrinyi, N., Pham, A.L.T., 2017. Oxidation of benzoic acid by heat-activated persulfate: effect of temperature on transformation pathway and product distribution. Water Res. 120, 43–51.